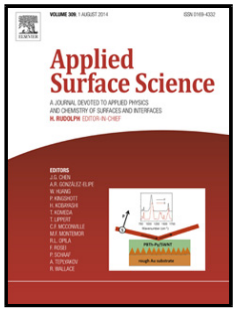

Title: Influence of Zr alloying on the mechanical properties, thermal stability and oxidation resistance of Cr-Al-N coatings

Author: W.Z. Li Q.Z. Chen T. Polcar R. Serra A. Cavaleiro

PII: S0169-4332(14)01865-0
DOI: http://dx.doi.org/doi:10.1016/j.apsusc.2014.08.115
Reference: APSUSC 28570

To appear in: *APSUSC*

Received date: 12-4-2014
Revised date: 27-7-2014
Accepted date: 20-8-2014

Please cite this article as: W.Z. Li, Q.Z. Chen, T. Polcar, R. Serra, A. Cavaleiro, Influence of Zr alloying on the mechanical properties, thermal stability and oxidation resistance of Cr-Al-N coatings, *Applied Surface Science* (2014), http://dx.doi.org/10.1016/j.apsusc.2014.08.115

Highlights

Addition of Zr to sputtered Cr-Al-N coatings can change the N stoichiometry.

Fcc (Cr, Zr)N phases in the low Zr coatings are stable up to 900 ^{o}C annealing.

Zr decreases the onset oxidation temperature of Cr-Al-Zr-N coatings.

Wear rate and friction coefficient increase significantly for the high Zr coatings.

Influence of Zr alloying on the mechanical properties, thermal stability and oxidation resistance of Cr-Al-N coatings

W.Z. Li*[a, b], Q.Z. Chen [a], T. Polcar [c], R. Serra [b], A. Cavaleiro*[b]

[a] School of Materials Science and Engineering, Guangxi University, Nanning 530004, PR China

[b] SEG-CEMUC - Department of Mechanical Engineering, University of Coimbra, Rua Luís Reis Santos, P-3030 788 Coimbra, Portugal

[c] National Centre for Advanced Tribology at Southampton (nCATS), School of Engineering Sciences, University of Southampton, Highfield, Southampton, SO171BJ, Hampshire, UK

Corresponding author. Tel.: +86 771 3270152; fax: +86 771 3270152

E-mail address: albano.cavaleiro@dem.uc.pt (A. Cavaleiro), wz-li@hotmail.com (W.Z. Li).

Abstract

Cr-Al-N coatings with Zr alloying (Zr contents from 0 to 29.5 at.%) were deposited by d.c. reactive magnetron sputtering. The chemical composition and the morphology of as-deposited coatings were characterized, and the phase structure, mechanical properties and wear resistance of the coatings before and after thermal annealing were analyzed and evaluated. With the increase of Zr content, both Cr and N contents decrease whereas Al shows a growing trend. Low Zr (< 26.9 at.%) coatings are stoichiometric and present a fcc NaCl-type B1 structure with columnar morphology, while high Zr (≥ 26.9 at.%) coatings are in N deficiency and have low crystallinity degree. The alloying of low contents of Zr improves the coating hardness and H/E ratio; however, for low ordered coatings these properties decrease significantly. After thermal annealing, fcc structure is kept in low Zr films whereas the crystalline degree is improved in the high Zr ones and

their mechanical properties were slightly improved. Two coatings were selected for further testing, representatives of low (CrAlZr5N) and high (CrAlZr27N) Zr contents. The onset oxidation temperature is ~ 900 ^{o}C and 600 ^{o}C for CrAlZr5N and CrAlZr27N coatings, respectively. Mainly Cr_2O_3 is formed on low Zr coatings whereas mixed oxides of ZrO_2 and Cr_2O_3 are detected on CrAlZr27N sample after thermal exposure. In all tribological tests, low Zr coating presents lower wear rate than the CrAlZr27N coating. In general, the addition of very high Zr contents (>20at.%) with N deficiency markedly weakens the mechanical properties and the oxidation resistance of Cr-Al-Zr-N coatings.

Keywords: Cr-Al-(Zr-)N coatings; Mechanical properties; Thermal stability; Wear resistance; Oxidation resistance

1. Introduction

Cr-N binary coatings have been widely used in many applications due to a good balance among wear, corrosion and mechanical properties [1, 2]. Alloying of Al element into coatings can further improve their mechanical properties and oxidation resistance [3, 4]. Lin et al. [3] found that the onset oxidation temperature and hardness were increased about 50~100 ^{o}C and 2~15 GPa, respectively, depending on the content of Al in the coating as compared to the binary system. Reiter et al. [5] demonstrated that, with the addition of Al, thermal stability, wear, and oxidation resistance of Cr-Al-N coatings could be effectively improved. The $Cr_{1-x}Al_xN$ coating with x=71 at.% exhibited the most desirable mechanical properties and the best tool life in drilling tests.

Another transition metal nitride, Zr-N coating has also attracted more and more interest as protective coating because of high hardness, and strong resistance to corrosion and wear [6, 7].

Furthermore, zirconium is often added to nitride coatings to improve their mechanical properties and corrosion resistance. Investigation by Zhang et al. [8] verified the positive effect of Zr alloying on the improvement of corrosion resistance of the Cr-N coatings. Kim et al. [9, 10] found that the incorporation of Zr could enhance the coating hardness and wear resistance, and decrease the surface roughness. However, the rapid formation of ZrO_2 on the coating surface strongly limits high temperature wear resistance. Considering the high thermal stability and strong oxidation resistance of Cr-Al-N coatings, it has been suggested that the introduction of Zr into the Cr-Al-N coating might tune the performance at high temperature. The study of Rojas et al. [11] showed that Cr-Al-Zr-N coating with 2 at.% Zr doping presented higher hardness and slightly weaker oxidation resistance than the Zr-free ternary nitride coatings. However, the effect of Zr, in a larger range of contents, on the mechanical properties and oxidation resistance of Cr-Al-Zr-N coating is still unclear. Furthermore, the high temperature mechanical properties and the wear resistance of such coatings have not still been investigated.

The present work, therefore, aims to study Cr-Al-Zr-N coatings deposited with different Zr contents with respect to the change of structure, and mechanical properties during thermal annealing in protective atmosphere and of wear resistance after thermal exposure. The high temperature properties and oxidation resistance of the coatings will be analyzed and evaluated.

2. Experimental

Cr-Al-(Zr-)N coatings were deposited by d.c. reactive magnetron sputtering technique in a multi-cathodes system with four rectangular magnetrons working in unbalanced mode; details can be found elsewhere [12]. In order to reduce the impact of substrates on the coating properties'

measurement, different materials were used as substrates, including M2 steel (Chemical composition (wt.%): W 6.4; Cr 4.2; Mo 5.0; V 1.9; C 0.9; Mn <0.4; Si <0.4; the balanced Fe) for mechanical properties measurement and thermal stability evaluation, (111) silicon for chemical composition and thickness evaluation and polycrystalline Al_2O_3 slices (dimensions 12 x 10 x 0.5 mm) for high temperature oxidation test. The substrate materials were ultrasonically cleaned in acetone and in alcohol for each 15 min, respectively. Before deposition, the pressure in the chamber was less than 2 x 10^{-4} Pa and Ar+ ion bombardment was used with a bias voltage of -400 V for 20 min to etch the sample surface. In order to enhance coating adhesion, a Cr interlayer thick ~ 200 nm was firstly deposited. During coating deposition, power density for Cr target and Al target was fixed as 2.25 W/cm^2, whereas 0, 1.5, 4.5, 6 or 7.5 W/cm^2 was used for Zr target. (Here the coating deposited at 3.0 W/cm² Zr target power density was not present, due to the structure and properties was very similar to that of 1.5 W/cm² Zr target power density). Gas flows of Ar 35 sccm and N_2 48 sccm were always kept, and the deposition time was 180 min.

Thermal annealing was performed at 900 ^{o}C in 95% Ar + 5% H_2 atmosphere for 1h to evaluate the coatings thermal stability. Thermogravimetric analysis (TGA) was conducted to determine the coating onset oxidation temperature by exposing the samples to industrial air (99.995% purity) in a TGA equipment. The final temperature was a very high temperature, 1200 ^{o}C with a heating rate of 10 ºC/min in order to understand the reaction during heating. The samples were then held at 1200 ^{o}C for 1h. Isothermal oxidation resistance tests were performed at 900 ^{o}C for 2 h with a heating rate of 30 ºC/min in the same TGA equipment.

The coating thickness was measured by profilometry, and the corresponding deposition rate was calculated dividing it by the deposition time. Cross-sectional and surface morphologies of the

coatings, as-deposited and after thermal exposure, were observed by scanning electron microscopy (SEM) and atomic force microscopy (AFM). Elemental content of the coating and elemental distribution along cross section of the exposed samples were detected by electron probe microanalysis (EPMA) and energy dispersive X-ray (EDX), respectively. The coating structure was determined by X-ray diffraction (XRD) with Co Kα radiation (λ = 0.178897 nm) in grazing mode (2°). The hardness (H) of the coating was measured by depth sensing nanoindentation and determined by Oliver and Pharr method [13]. The applied load was 10 mN and 12 measurements were done in each sample. Why 10 mN applied load was selected is to guarantee the best compromise to test the highest depth of coatings material without having substrate influence, for the thinnest coating, and to avoid the influence of indentation size on the hardness values for thicker coatings. The adhesion of the coatings, before and after thermal annealing, was evaluated by scratch testing. The critical load L_c was determined by analyzing the scratch track by optical microscopy. The wear resistance of the coating under different conditions was evaluated by pin-on-disk tests. The friction coefficient and the wear rate were determined with a normal applied load of 5 N, sliding speed of 5 cm/s and 5000 laps, and an Al_2O_3 ball as a counterpart (6 mm in diameter. Al_2O_3 ball is stable in the structure and properties under different testing temperatures, so as to avoid as much as possible the interference of the ball on the tribological behavior of the sample). The value of the wear rate was calculated by dividing the worn volume (integrating the cross-profile of the track to the entire worn circle) by the applied load and the total distance.

3. Results and discussion

3.1. Chemical composition, deposition rate and microstructures

The chemical composition of the as-deposited coating on (111) silicon wafer is listed in Table 1. As expected, Zr content increases nearly linearly from 0 to 29.5 at.% with the increase of Zr target power density from 0 to 7.5 W/cm^2, whereas Cr content shows an inverse trend, from 33.8 at.% down to 17.4 at.%. Aluminum shows a quite peculiar behavior: for low Zr contents Al slowly decreases with increasing Zr target power density and, then, suddenly jumps to 22.4 at.% and 22.8 at.% for high Zr content. This sudden variation is accompanied with a sharp decrease of N content. The increasing total power applied to the targets impedes their complete poisoning with the discharge switching from compound to metallic mode, with the consequent decrease in the nitrogen percentage in the deposited films. Such a discharge mode is also influencing significantly the deposition rate, which increases from rather low values of about 10~14.7 nm/min in low Zr coatings up to ~ 44.4 nm/min, when Zr target power density is 6 W/cm^2 (Fig. 1)). This is a clear indication of insufficient poisoning of the target with the consequent much higher sputtering yield of the metallic elements. Similar trends of chemical composition and deposition rate were studied in detail and interpreted in previous paper [12].

Figure 2 shows cross-sectional SEM and surface AFM morphologies of the coatings on (111) silicon wafer. A columnar structure is typical of low Zr coatings (Fig. 2(a, b, c)). In high Zr coatings, mixed morphologies of columnar overlayer and featureless sublayer are observed (Fig. 2(d)). AFM corroborates the cross section observations. The size of the globular relief features is in a range of 100~250 nm and decreases with Zr content in low Zr coatings in agreement with less and less defined columns in SEM cross section micrographs. In the high Zr coatings (Fig. 2(d)), the dimension of the surface bumps increases. The surface roughness is in accordance, rather low about 5~10 nm for low Zr coatings and much higher 35~40 nm for CrAlZr30N coating.

3.2. Thermal stability

To investigate the coating thermal stability, coating samples were annealed at 900 ^{o}C for 1h in protective atmosphere. Figs. 3(a, b) show the XRD patterns of the coatings before and after thermal annealing. In the as-deposited coatings, only NaCl type fcc phases (Cr, Zr)N are detected (Fig. 3(a)). With the increase of Zr in the coatings, the diffraction peaks shift to lower angles, from those close to CrN phase (ICDD 11-0065) to those of ZrN phase (ICDD 35-0753). The calculated lattice parameter from the (111) diffraction peak confirms an almost linear increase in the lattice parameter from the Zr-free coating up to the highest Zr coating (Fig. 3(c)), suggesting the progressive substitution of Cr(Al) atoms by bigger Zr atom (0.206 nm in atomic radius compared to 0.166 nm and 0.118 nm for Cr and Al atoms, respectively [14]). The lattice distortion induced by the Zr substitution gives rise to a decrease in the crystal order, as suggested by the significant decrease in the grain size calculated by the Scherrer's equation (Fig. 3(c)). After thermal annealing, only the fcc structure is detected in low Zr coatings (Fig. 3(b)). However, in high Zr coatings, besides the residual oxide formed at ~36° and ~59°, a strong new peak can be detected at ~52º, which can be attributed to metallic Cr (ICDD 85-1336). The lower affinity of Cr for N in comparison to Zr and Al [15], and the low N content in relation to a stoichiometric FCC nitride, makes the precipitation of Cr phase possible. Globally, the crystalline degree is improved compared to the as-deposited state, with grain growing after annealing (Fig. 3 (c)).

Figure 4 shows the hardness, H/E and H^3/E^{*2} of the coatings before and after thermal annealing. H and E are the hardness and Young's modulus, respectively. E* is the effective Young's modulus: $E^*=E / (1-\nu)$ and ν, the Poisson rate, equals to 0.25. The trend for hardness, H/E and H^3/E^{*2} is similar, regardless of as-deposited or thermal annealed condition. They increase first

and, then, decrease with the increase of Zr in the coatings. The first trend can be attributed to a solid solution hardening related to the incorporation of Zr atoms in solid solution of the fcc mixed nitride phase [12]. The strong lattice distortion induced by the bigger Zr atoms interferes in the deformation process increasing significantly the materials strength. The lower hardness and H/E or H^3/E^{*2} ratios reveal the metallic character of the high Zr coatings. The N deficiency in relation to stoichiometric nitrides and the extremely reduced grain size (inverse Hall-Petch relationship [16]) of these coatings are possible explanations for the hardness reduction. Annealed samples are always harder compared to as-deposited coatings. In spite of the good global thermal stability of the coatings, the occurrence of several softening effects, such as reduction in lattice distortion, small grain growth, metallic Cr precipitation and surface oxidation (the last two effects only in high Zr coatings) should induce a decrease in the hardness of annealed coatings. However, there is a countercurrent effect that can justify the small observed improvements in this property, the residual stresses. Any of the possible nitrides, AlN, CrN and ZrN, have thermal expansion coefficients much smaller than the substrate M2 steel used in the samples for hardness measurement. We think that the coefficient for the mixed nitride should be of this order too. Therefore, compressive residual stresses should be created in the coatings when cooling down from the annealing temperature due to the mismatch between the thermal expansion coefficients of the coating and the substrate. The high H/E and H^3/E^{*2} ratios found for coatings with low Zr additions, particularly after thermal annealing, make envisaging interesting tribological and/or toughness properties for these coatings [17, 18].

Scratch test is a simple and practical method to evaluate coating cohesion/adhesion properties [19]. Sometimes critical loads from the coating first cracking and peeling off or substrate exposure

during scratching are used to assess the coating toughness [20]. The coatings were scratched by a Rockwell C indenter before and after thermal annealing; the corresponding results are shown in Table 1. The arrows in Fig. 5 point out the positions of coating failure during scratch testing. The critical loads L_{c2} and L_{c3} denotes the coating edge chipping and substrate exposure, respectively. No substrate exposure was found in the low Zr coatings in the as-deposited condition (Fig. 5(a)). With the increase of Zr content, the as-deposited coating exhibits decreased resistance to edge chipping or coating spallation. By comparison, the coating after thermal annealing is easily damaged during scratching. The substrate exposure was detected in all samples. Fig. 5 shows the typical scratch track morphologies of CrAlZr5N and CrAlZr27N coatings before and after thermal annealing. Edge chipping or substrate exposure cannot be found in the as-deposited CrAlZr5N coating (Fig. 5(a)) during scratching up to 75N load. However, substrate exposure was detected in the annealed sample (Fig. 5(b)) when the load was 55N. In CrAlZr27N coating, large area edge chipping and substrate exposure were evident in both as-deposited and annealed cases (Fig. 5 (c-f)). During scratching tests, hardly any first cracking (L_{c1}) was detected, except for the CrAlZr30N coating. It is, thus difficult to evaluate the coating toughness by Scratch Crack Propagation Resistance (CPRs= $L_{c1}(L_{c3}- L_{c1})$) [20].

3.3. Oxidation resistance

Onset oxidation temperature of the coating was investigated by exposing the coatings to air in TGA equipment. Figure 6(a) displays the curves of mass gain of the coating with increasing temperature up to 1200 ^{o}C. It is found that the onset oxidation temperature is relatively high, above 950 ^{o}C in the Zr-free coating. The XRD results show that Cr_2O_3 phase is formed on the coating after 1h exposure at 1200 ^{o}C (Fig. 6(b)). With the introduction of 5 at.% Zr, the coating

starts to oxidize at ~ 900 ^{o}C (Fig. 6(a)). In addition to Cr_2O_3, ZrO_2 is also detected (Fig. 6(b)). For CrAlZr27N coating, a significant increase in the mass gain is found around 600 ^{o}C (Fig. 6(a)). A sudden drop at 1150 ^{o}C was thought to be caused from a fast spallation of Zr oxides due to their high growth rate and volume expansion [21]. XRD results indicate that ZrO_2 phases (both monoclinic and tetragonal) are the main oxidation product instead of Cr_2O_3 (Fig. 6(b)) observed in low Zr coating.

In order to evaluate appropriately oxidation resistance, the CrAlZr5N and CrAlZr27N coatings were thermally exposed to 900 ^{o}C in industrial air for 2h . The variation of mass gain with exposure time is shown in Fig. 7(a). CrAlZr5N coating exhibits a rather slow increase in mass gain with exposure time (~ 0.12 mg/cm^2 for 2h exposure), which should be attributed to the formation of a protective oxide scale on the top surface of the coating. For the high Zr coating, a very rapid increase up to 0.84 mg/cm^2 is found in the first ~20 min, followed by an abrupt drop and, then, a low increase. As it would be expected from the oxidation results up to 1200 ºC (Fig. 6(a)), in the first part of the curve a high oxidation rate takes place, producing a thick oxide scale. The sudden decrease in the weight gain should be attributed to the partial flaking of the oxide scale, which fell down from the sample holder. The third part of the curve corresponds to the final oxidation of the very low remaining portion of the as-deposited coating, overlapped by the inert behaviour of the alumina substrate.

SEM image of oxidized surface shows oxide particles distributed on the CrAlZr5N coating (Fig. 7(b)). The cross-sectional image shows that cubic (Cr, Zr)N nitrides are still present in the sample and the oxide layer is quite dense and featureless (Fig. 7(c)). XRD detection proved that the scales are composed mainly of Cr_2O_3. On the CrAlZr27N coating (Fig. 7(d)) oxide flakes can

be observed, which should be the remnants after the scale spallation. EDS analysis indicates that these flakes are Zr-rich mixed-oxides (Zr 13.5at%, Cr 9.7at%, Al 12.2at% and O 64.6at%). The fracture cross-sectional image (Fig. 7(e)) suggests that the coating is fully oxidized. Due to their high thermal stability, slow-growth and high density, Cr_2O_3 or Al_2O_3 are thought to be ideal surface scales to protect the underlying materials from oxidation attack [22], whereas ZrO_2 seems to be non-protective and, further, it is easy spalled from the surface [21]. Therefore, the introduction of high Zr content into the coating will weaken the oxidation properties regardless of a high Al content, since continuous Al_2O_3 scales are not formed on the coating surface during thermal exposure.

3.4. Tribological behavior

Globally, the coatings studied in this work could be split into two main groups with similar mechanical properties and oxidation resistance: the films with low (up to 20 at.%) and high Zr content. Therefore, CrAlZr5N and CrAlZr27N coatings were selected for further studies concerning tribological behavior at room temperature (RT) and at 700 ºC evaluated by pin-on-disk testing. Moreover, sliding tests were also performed on the sample tested at 700 ºC after it has been cooled down to RT. To select 700 ºC for high temperature testing is based on, (i) this temperature is very close to the upper limit of the testing equipment (800 ºC), allowing a better reliability of the test; (ii) it is well known that the real temperature in the contact can be hundreds of ºC higher than the testing temperature what, in case of using higher testing temperatures, could lead to a premature destruction of the coatings. Figure 8 and Fig. 9 show the friction coefficient, the wear track profile and the surface morphology of both coatings. Friction coefficient is ~ 0.5 - 0.6 for CrAlZr5N coating (Fig. 8(a)) tested at room temperature before and after annealing value

very similar to that of CrAlN coating tested under the same conditions [23]; there was almost no change in friction when comparing as-deposited and annealed samples. The wear track profiles are very shallow, with depth ~ 350 nm (Fig. 8(b)). Testing at 700 ºC resulted in maximum depth of the wear track 5.6 μm indicating complete removal of the coating. The wear rate is about 2.8 x 10^{-6} mm^3/Nm for 700 ^oC test, which is equivalent to that of Zr-free coating tested at 500 ^oC [23]. The value of the wear rate is ~ 0.22 x10^{-6} mm^3/Nm and 0.34 x10^{-6} mm^3/Nm for coating tested at RT and RT after 700 ºC, respectively. CrAlZr27N coating presents worse tribological performance either for the friction or the wear coefficients. In all the three testing conditions the COF is about 0.7 - 0.8. Again, for the 700 ^oC test a higher scattering of the COF values is obvious (Fig. 9(a)). The simultaneous analysis of Fig. 9(b) and (d) shows that an abrupt step is observed in the border of the tracks, suggesting the flaking of the coating. The measurement of the depth gives a value close to 8 μm, which is the thickness of the coating. In the center of the wear track, the depth increases meaning that substrate is contributing for the friction behavior, explaining the oscillations in the friction curve. The wear tracks of the coatings tested at room temperature are considerable wide and deep (Fig. 9(b, c)) in comparison to those of low Zr coating. However, the maximum measured depths less than 7.0 μm reveal that the coatings were not completely worn through. The wear rate is about 50 x10^{-6} mm^3/Nm and 27 x10^{-6} mm^3/Nm for the RT and RT after 700 ºC tests, respectively, which are typically two orders of magnitude higher than those found for low Zr coating.

Combining these results with those of our previous research in Zr-free coating [23], it can be suggested that the introduction of low Zr content can improve the wear resistance of CrAlN coating at room temperature, to a certain extent, although this improving effect declines at high

temperature. On the other hand, the presence of high Zr contents markedly weakens the coating mechanical properties and its tribological performance.

4. Conclusions

CrAlN coatings alloyed by Zr with the content from 0 to 29.5 at% were deposited by d.c. reactive magnetron sputtering. With the increase of Zr content, Cr and N contents decreased, and Al first decreased and then increased. Low crystalline order degree and N deficiency were observed when high Zr contents were introduced. After thermal annealing, low Zr coatings kept the fcc structure while high Zr coatings improved the crystallinity. The hardness, toughness, H/E and H^3/E^{*2} first increased and then decreased as Zr increased in the as-deposited coatings; after annealing, globally all of them improved the hardness. Moreover, the coatings after annealing experienced a decrease in the resistance to scratching.

The onset oxidation temperature was ~ 900 ^oC and 600 ^oC for CrAlZr5N and CrAlZr27N coating, respectively. The stronger oxidation resistance of Zr-free and low Zr coatings is due to the formation of Cr_2O_3 scales instead a mixture of Cr_2O_3 and ZrO_2.

Low COF ~ 0.5 - 0.6 was registered for CrAlZr5N in comparison to 0.6 - 0.8 for CrAlZr27N coating. Under all different testing conditions (RT, 700 ^oC or RT after 700 ^oC/1h annealing) similar tribological performance was observed in relation to the wear rate. The introduction of high Zr with N deficiency is detrimental to the mechanical properties and the oxidation resistance of CrAlN coatings.

Acknowledgements

This work was supported by the Portuguese Foundation for Science and Technology (FCT, SFRH/BPD/76925/2011), the National Natural Science Foundation of China (Grant No. 51371059, 51001032 and 51361003), Guangxi Science Foundation (Grant Nos. 2014GXNSFCA118013 and 0731013), Guangxi Natural Science Fund for Innovative Research Team (Grant No. 2011GXNSFF018001), and Guangxi BAGUI Scholar Program, which are gratefully acknowledged. The authors are grateful to Nelson Santos Duarte from IPN at Coimbra for the XRD analysis.

References

[1] S.K. Pradhan, C. Nouveau, A. Vasin, M.-A. Djouadi, Surf. Coat. Technol., 200 (2005), pp. 141-145

[2] W.Z. Li, Q.M. Wang, J. Gong, C. Sun, X. Jiang, Appl. Surf. Sci., 255 (2009), pp. 8190-8193

[3] J. Lin, B. Mishra, J.J. Moore, W.D. Sproul, Surf. Coat. Technol., 202 (2008), pp. 3272-3283

[4] J.E. Sanchéz, O.M. Sanchéz, L. Ipaz, W. Aperador, J.C. Caicedo, C. Amaya, M.A. Hernández Landaverde, F. Espinoza Beltran, J. Muñoz-Saldaña, G. Zambrano, Appl. Surf. Sci., 256 (2010) , pp. 2380-2387

[5] A.E. Reiter, V.H. Derflinger, B. Hanselmann, T. Bachmann, B. Sartory, Surf. Coat. Technol., 200 (2005), pp. 2114-2122

[6] G. Dorcioman, G. Socol, D. Craciun, N. Argibay, E. Lambers, M. Hanna, C.R. Taylor, V. Craciun, Appl. Surf. Sci., 306 (2014), pp. 33–36

[7] S.M. Aouadi, A. Bohnhoff, M. Sodergren, D. Mihut, S.L. Rohde, J. Xu, S.R. Mishra, Surf. Coat. Technol., 201 (2006), pp. 418-422

[8] Z.G. Zhang, O. Rapaud, N. Bonasso, D. Mercs, C. Dong, C. Coddet，Vacuum, 82 (2008), pp. 1332-1336

[9] G.S. Kim, B.S. Kim, S.Y. Lee, J.H. Hahn, Surf. Coat. Technol., 200 (2005), pp. 1669-1675

[10] S.M. Kim, B.S. Kim, G.S. Kim, S.Y. Lee, B.Y. Lee, Surf. Coat. Technol., 202 (2008), pp. 5521-5525

[11] T.C. Rojas, S. El Mrabet, S. Domínguez-Meister, M. Brizuela, A. García-Luis, J.C. Sánchez-López, Surf. Coat. Technol., 211 (2012), pp. 104-110

[12] W.Z. Li, M. Evaristo, A. Cavaleiro, Surf. Coat. Technol., 206 (2012), pp. 3764-3771

[13] W.C. Oliver, G.M. Pharr, J. Mater. Res., 7 (1992), pp. 1564-1583

[14] http://www.webelements.com/atom_sizes.html 2014-04-10

[15] I. Barin, Thermochemical Data of Pure Substances, VCH Verlagsgesellschaft mbH.,Weinheim, Third Edition, 1995

[16] C. Suryanarayana, Materials Today, 15 (2012), pp. 486-498

[17] A. Leyland, A. Matthews,Wear, 246 (2000), pp. 1-11

[18] J. Musil, M. Jirout, Surf. Coat. Technol., 201 (2007), pp. 5148-5152

[19] J. Stallard, S. Poulat, D.G. Teer, Tribol. Int., 39 (2006), pp. 159-166

[20] S. Zhang, D. Sun, Y.Q. Fu, H.J. Du, Surf. Coat. Technol., 198 (2005), pp. 74-84

[21] L.F. He, Y.W. Bao, M.S. Li, J.Y. Wang, Y.C. Zhou, J. Mater. Res., 23 (2008), pp.3339-3346

[22] J.R. Nicholls, MRS Bull., 28 (2003), pp. 659-670

[23] T. Polcar, A. Cavaleiro, Surf. Coat. Technol., 206 (2011), pp. 1244-1251

Figure captions

Fig. 1. Deposition rate of the coatings deposited with increasing Zr target power density.

Fig. 2. SEM fracture cross-sectional micrographs and AFM images of Cr-Al-(Zr-)N coatings on (111) silicon wafers: (a) CrAlN; (b) CrAlZr5N; (c) CrAlZr17N; (d) CrAlZr30N.

Fig 3. XRD patterns (a, b) and calculated grain size and lattice parameter (c) of the coatings on M2 steels as-deposited (a) and annealed at 900 ^{o}C in 95% Ar + 5% H_2 atmosphere for 1h (b). The XRD tests were done with Co Kα radiation (λ = 0.178897 nm) in grazing mode (2°). CrN (ICDD 11-0065), ZrN (ICDD 35-0753), Cr (ICDD 85-1336), *t*-ZrO_2 (ICDD 50-1089).

Fig. 4. Hardness, H/E and H^3/E^{*2} of the coatings on M2 steels as-deposited and after 900 ^{o}C annealing in 95% Ar + 5% H_2 atmosphere for 1 h. 10 mN applied load was used for depth sensing nanoindentation test.

Fig. 5. Typical scratch track morphologies of the coatings on M2 steels as-deposited (a, c, d) and after 900 ^{o}C annealing (b, e, f): (a, b) CrAlZr5N; (c, d, e, f) CrAlZr27N. 200 μm tip radius indenter, 100 N/min loading speed and 10 mm/min scratch speed. Scratch direction is from left to right. The arrows point out the positions of coating failure during scratching.Lc_2- edge chipping, Lc_3- substrate exposure.

Fig. 6. TGA curves (a) and XRD patterns (b) of the coatings on Al_2O_3 slices thermally exposed to 1200 ^{o}C in industrial air (99.995% purity) for 1h. The XRD tests were done with Co Kα radiation (λ = 0.178897 nm) in grazing mode (2°). Cr_2O_3 (ICDD 38-1479), *m*-ZrO_2 (ICDD 17-0923), *t*-ZrO_2 (ICDD 50-1089).

Fig. 7. TGA curves (a), SEM surface (b, d) and fracture cross-sectional micrographs (c, e) of the CrAlZr5N (b, c) and CrAlZr27N (d, e) coatings on Al_2O_3 slices after thermal exposure at 900

^{o}C in industrial air for 2h. Oxides are Cr-rich in (c) and Zr-rich in (e), respectively; Nitrides are (Cr, Zr)N phases in (c).

Fig. 8. Friction coefficient (a), wear track profile (b) and surface morphologies (c, d, e) of the CrAlZr5N coating on M2 steel testing under different conditions. 5 N normal applied load, 5 cm/s sliding speed and 5000 laps, and 6 mm Al_2O_3 ball as a counterpart.

Fig. 9. Friction coefficient (a), wear track profile (b) and surface morphologies (c, d, e) of the CrAlZr27N coating on M2 steel testing under different conditions. 5 N normal applied load, 5 cm/s sliding speed and 5000 laps, and 6 mm Al_2O_3 ball as a counterpart.

Table 1 Chemical composition, thickness, L_{c2}, L_{c3} and designated name of Cr-Al-Zr-N films.

Zr Target Power Density (W/cm^2)	Chemical composition (at.%)				Thickness (μm)	L_{c2} (N)		L_{c3} (N)		Designated name
	Cr	Al	Zr	N		As deposited	900 °C annealing	As deposited	900 °C annealing	
0	33.8	12.9	0	53.3	2.0	N/A	N/A	N/A	62	CrAlN
1.5	33.8	12.3	5.0	48.9	2.1	N/A	N/A	N/A	55	CrAlZr5N
4.5	23.9	10.4	16.5	49.2	2.9	49	N/A	N/A	58	CrAlZr17N
6	19.0	22.4	26.9	31.7	8.2	51	21	63	52	CrAlZr27N
7.5	17.4	22.8	29.5	30.3	8.8	26	29	42	43	CrAlZr30N

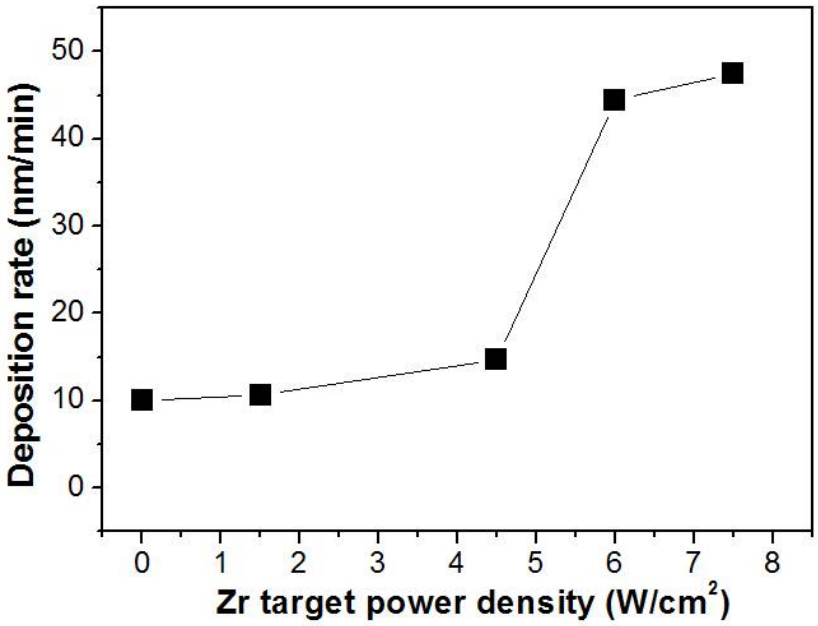

Fig. 1. Deposition rate of the coatings deposited with increasing Zr target power density.

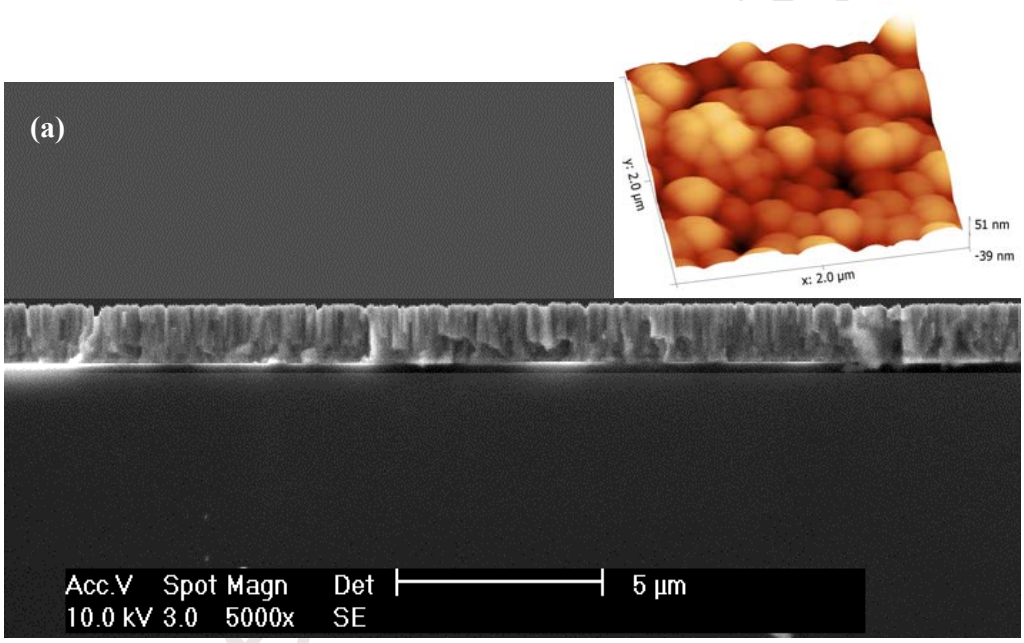

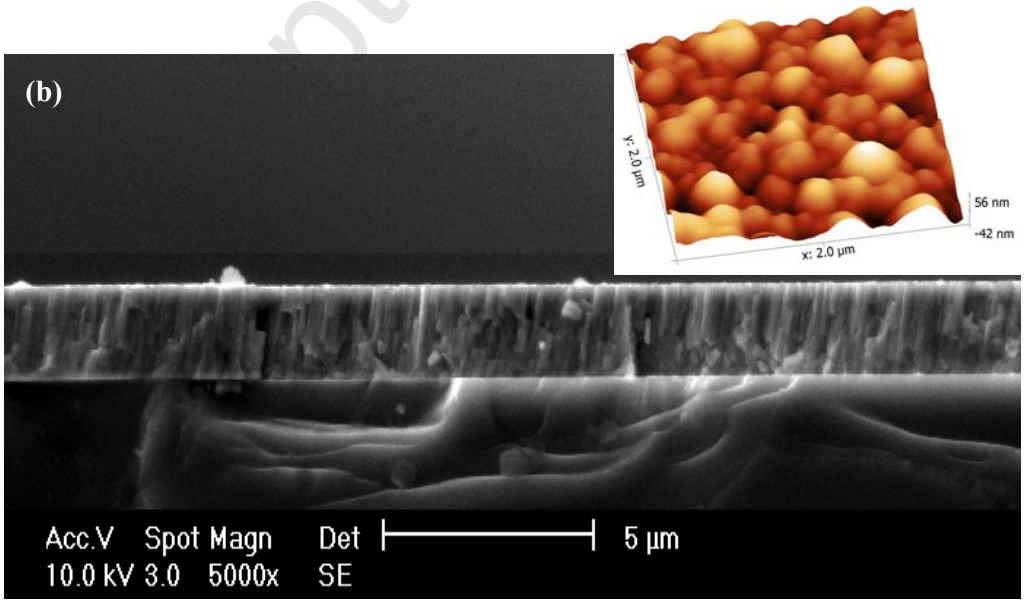

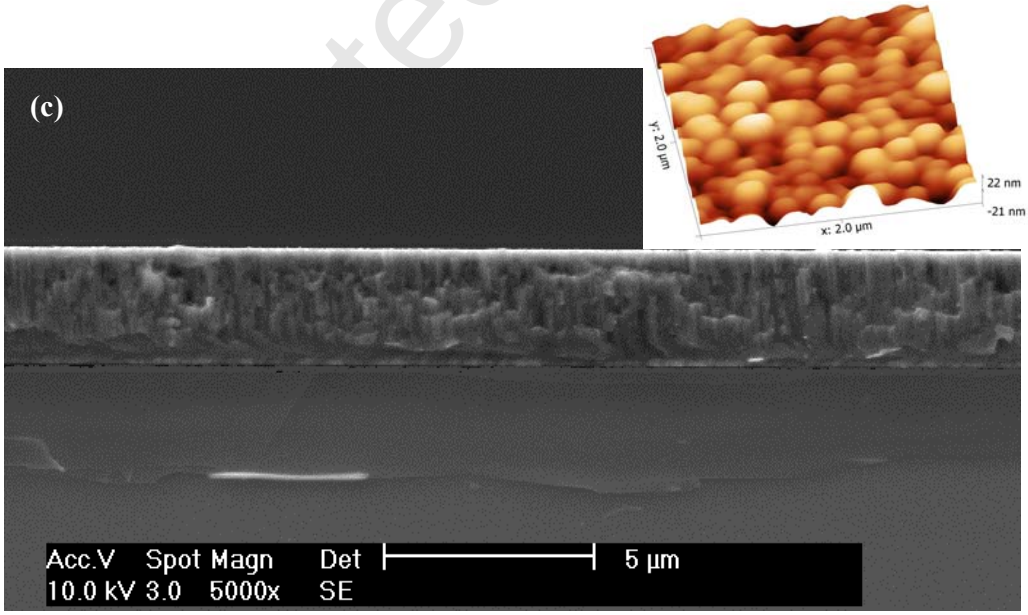

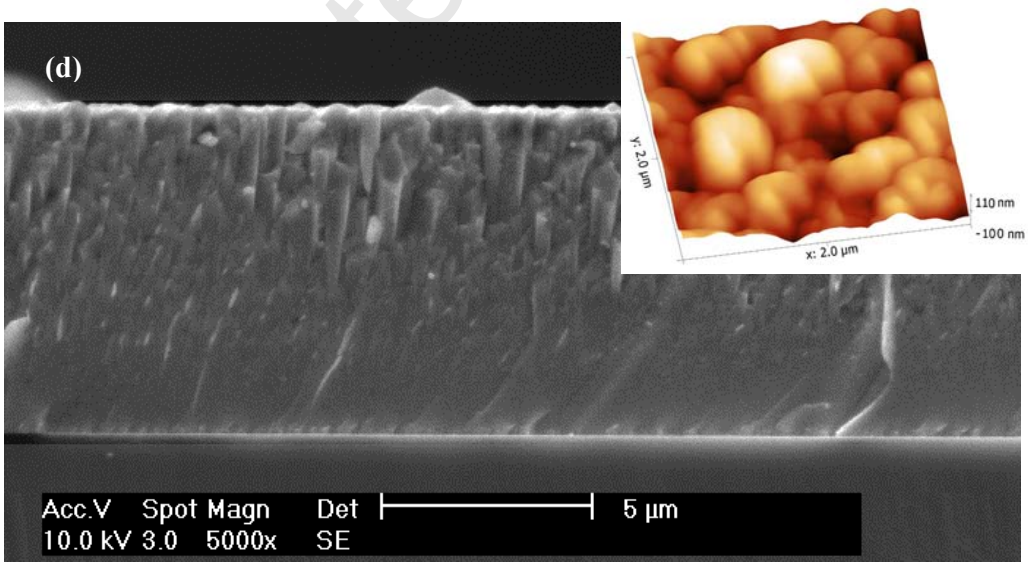

Fig. 2. SEM fracture cross-sectional micrographs and AFM images of Cr-Al-(Zr-)N coatings on

(111) silicon wafers: (a) CrAlN; (b) CrAlZr5N; (c) CrAlZr17N; (d) CrAlZr30N.

(a)

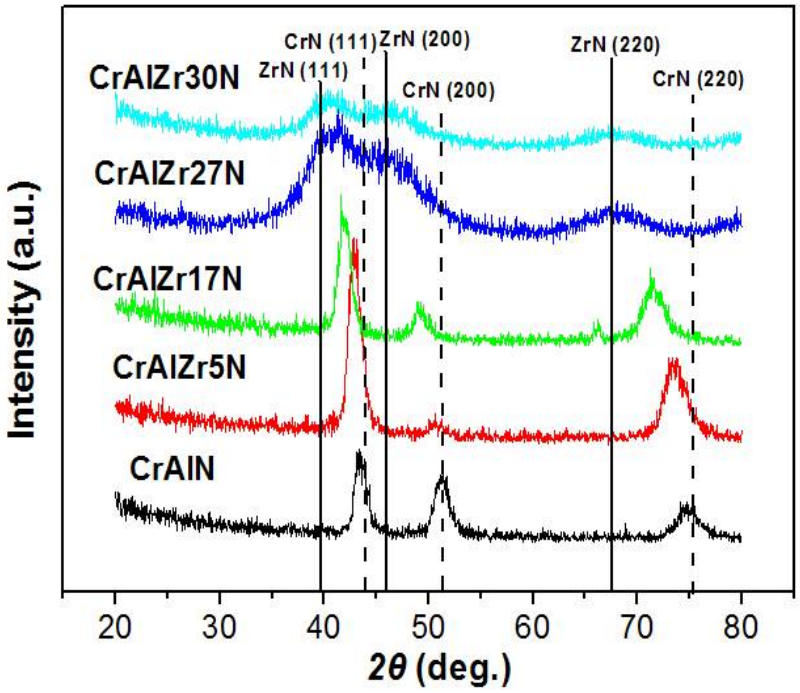

(b)

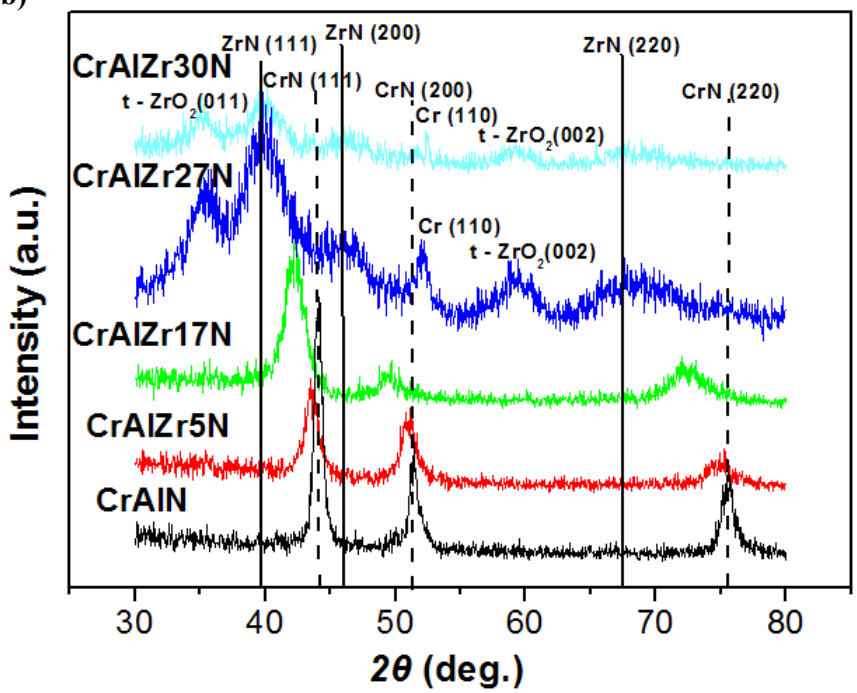

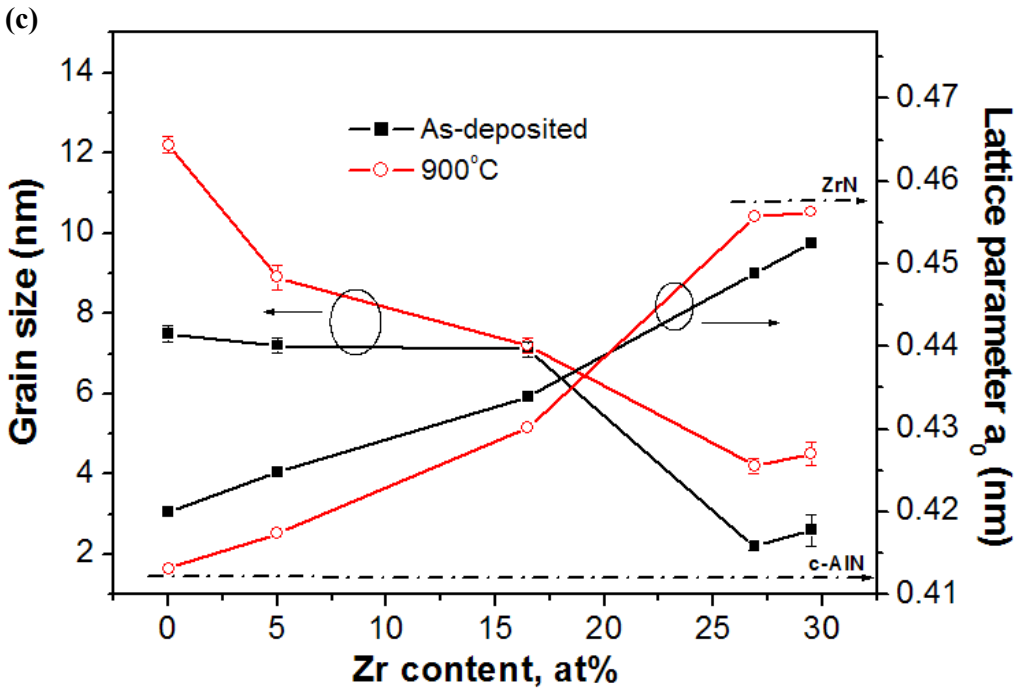

Fig 3. XRD patterns (a, b) and calculated grain size and lattice parameter (c) of the coatings on M2 steels as-deposited (a) and annealed at 900 ^{o}C in 95% Ar + 5% H_2 atmosphere for 1h (b). The XRD tests were done with Co Kα radiation (λ = 0.178897 nm) in grazing mode (2°). CrN (ICDD 11-0065), ZrN (ICDD 35-0753), Cr (ICDD 85-1336), *t*-ZrO_2 (ICDD 50-1089).

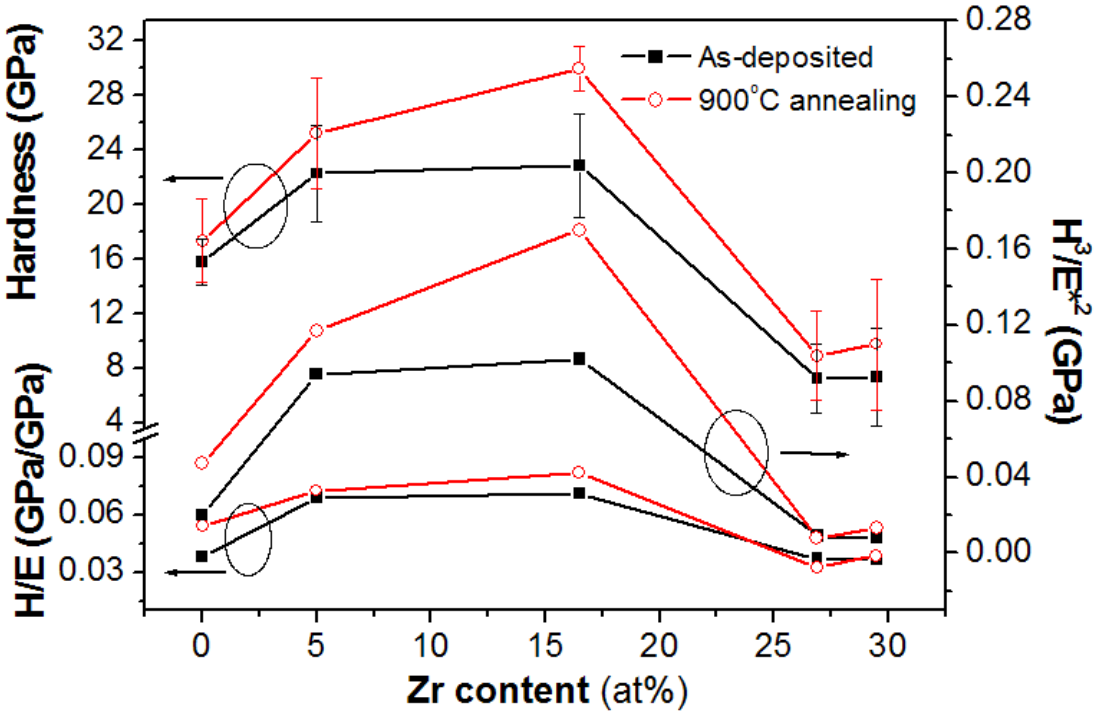

Fig. 4. Hardness, H/E and H^3/E^{*2} of the coatings on M2 steels as-deposited and after 900 ^oC annealing in 95% Ar + 5% H_2 atmosphere for 1 h. 10 mN applied load was used for depth sensing nanoindentation test.

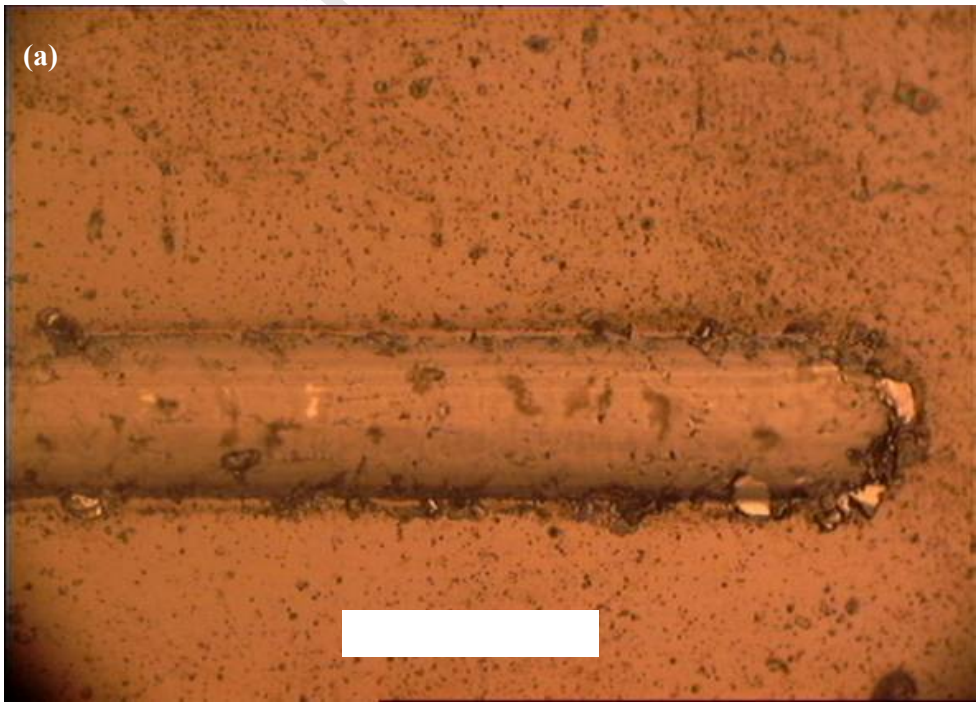

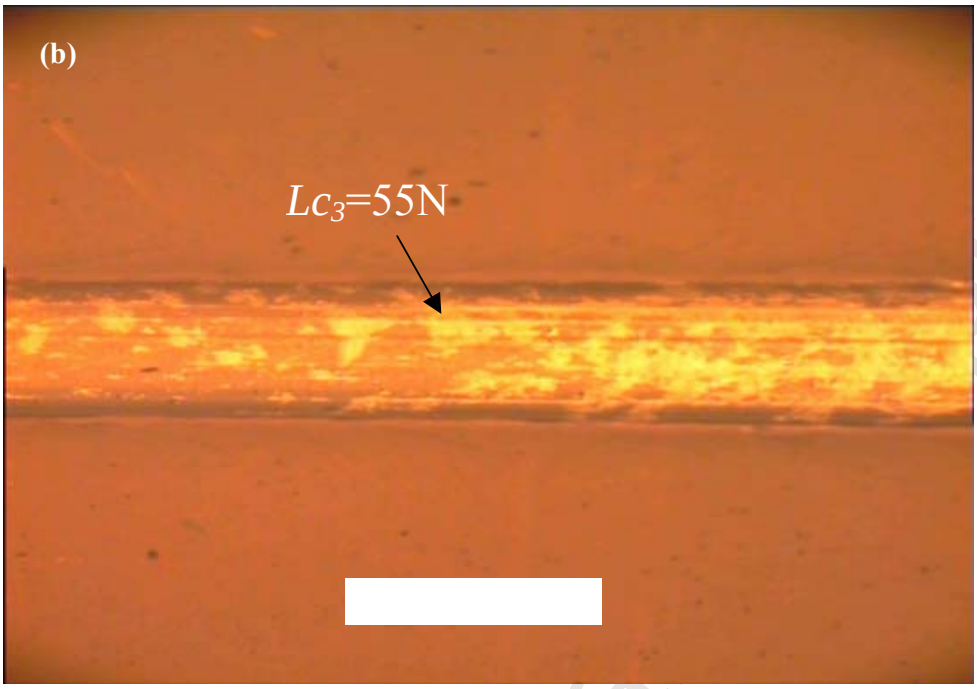

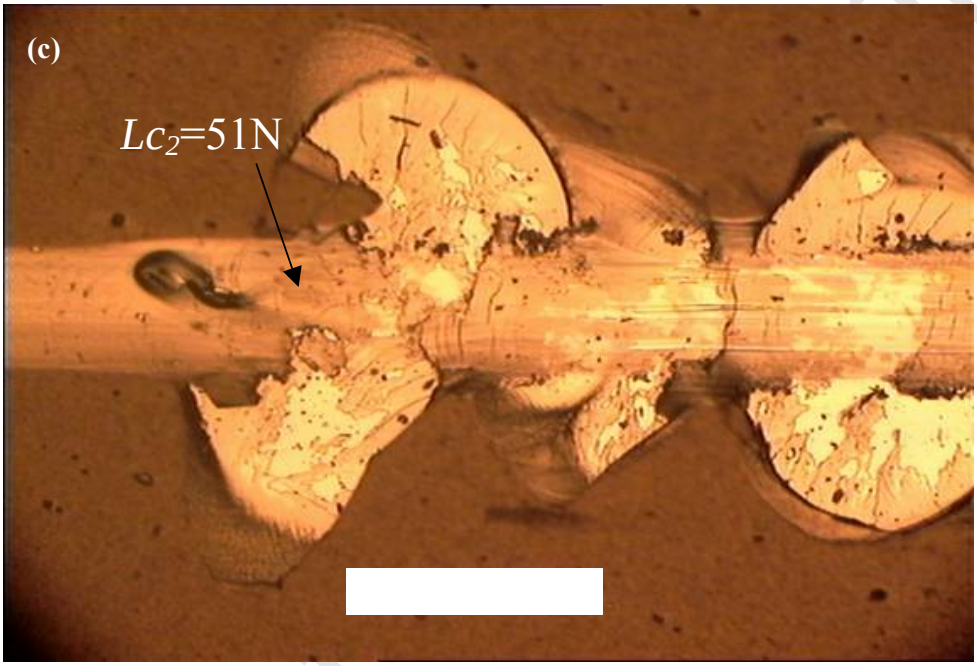

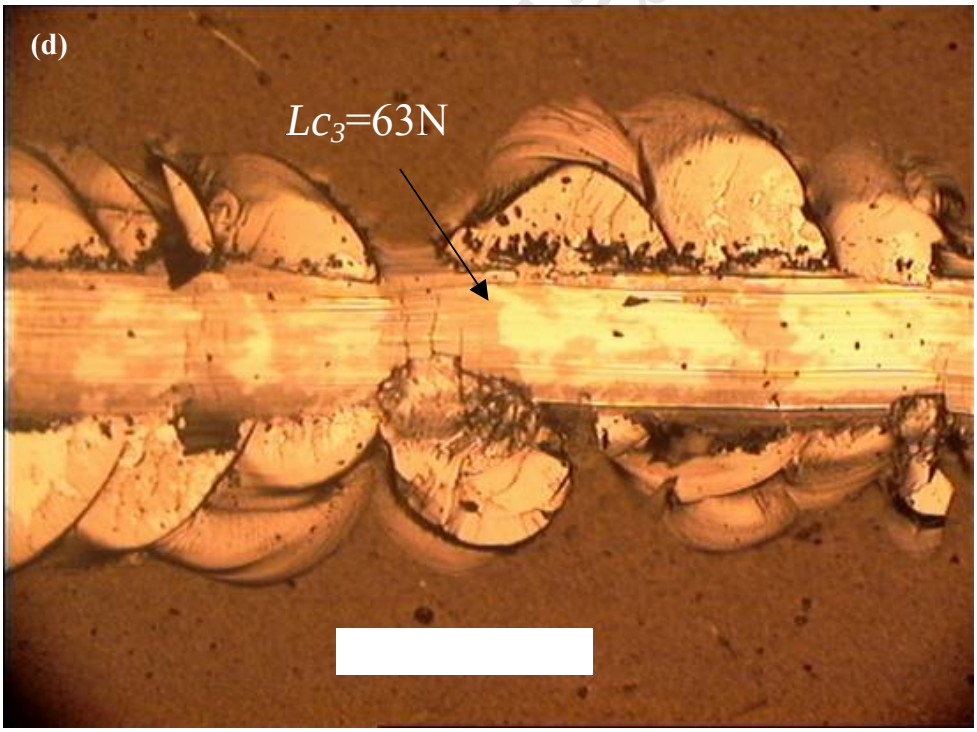

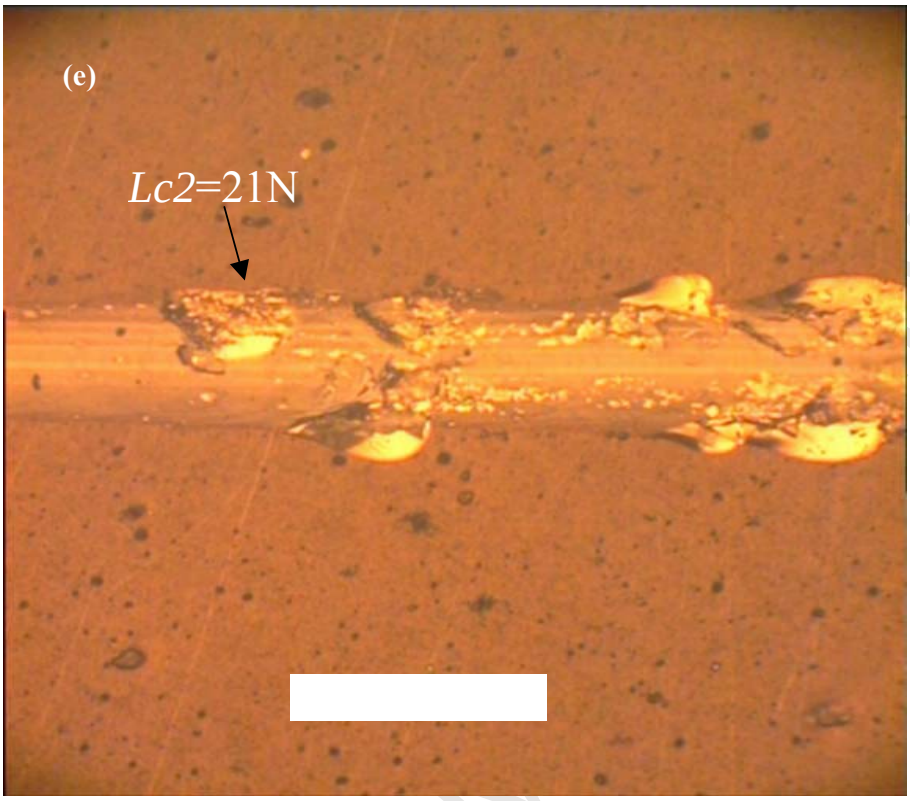

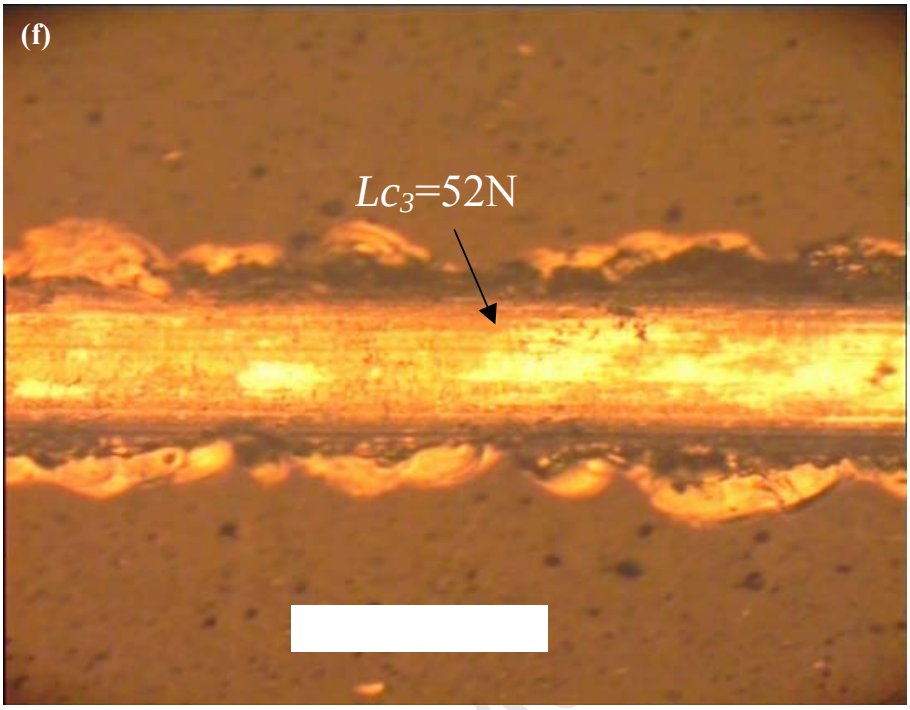

Fig. 5. Typical scratch track morphologies of the coatings on M2 steels as-deposited (a, c, d) and after 900 ^{o}C annealing (b, e, f): (a, b) CrAlZr5N; (c, d, e, f) CrAlZr27N. 200 µm tip radius indenter, 100 N/min loading speed and 10 mm/min scratch speed. Scratch direction is from left to right. The arrows point out the positions of coating failure during scratching. Lc_2- edge chipping, Lc_3- substrate exposure.

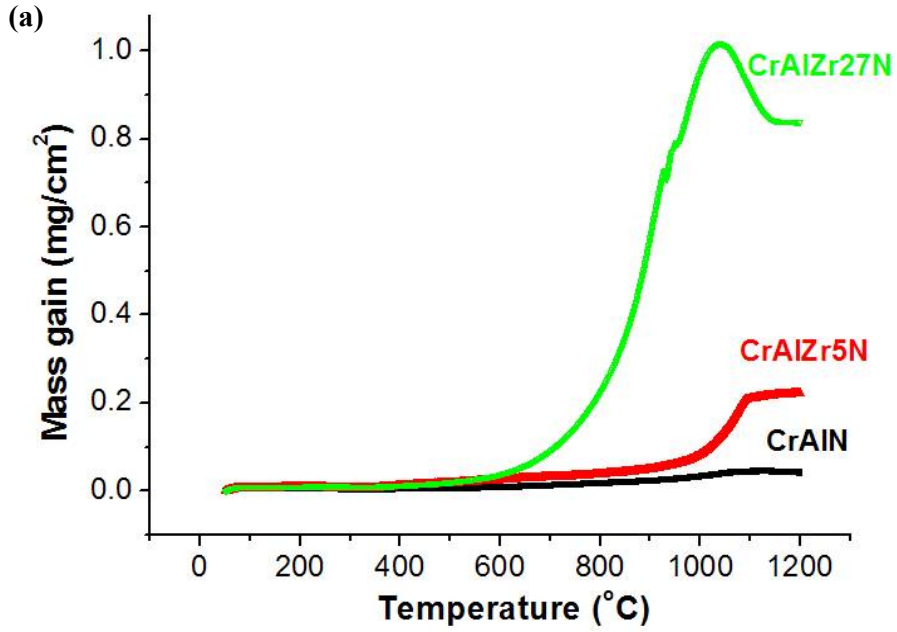

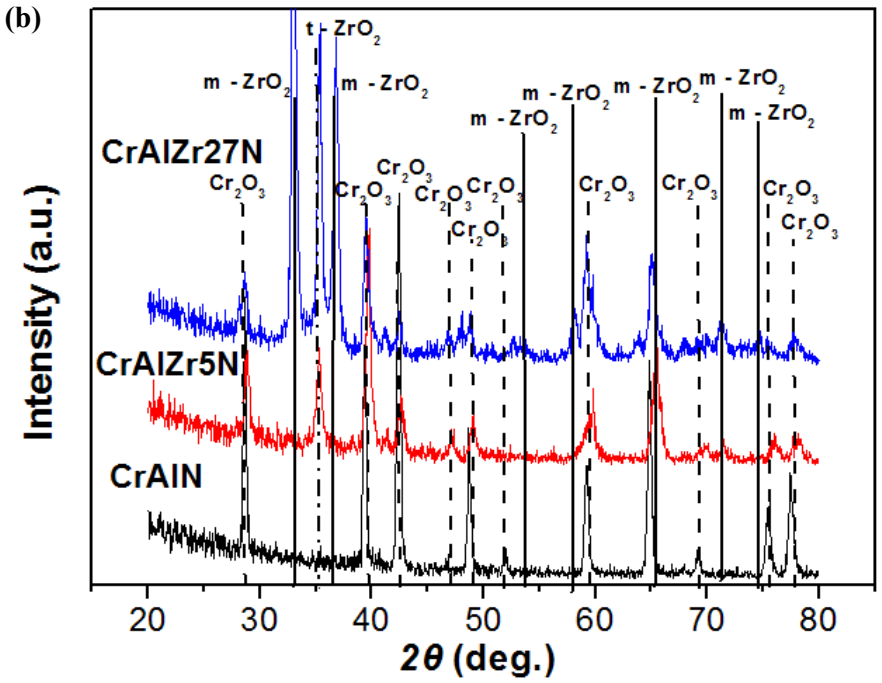

Fig. 6. TGA curves (a) and XRD patterns (b) of the coatings on Al_2O_3 slices thermally exposed to 1200 ^{o}C in industrial air (99.995% purity) for 1h. The XRD tests were done with Co Kα radiation (λ = 0.178897 nm) in grazing mode (2°). Cr_2O_3 (ICDD 38-1479), *m*-ZrO_2 (ICDD 17-0923), *t*-ZrO_2 (ICDD 50-1089).

(a)

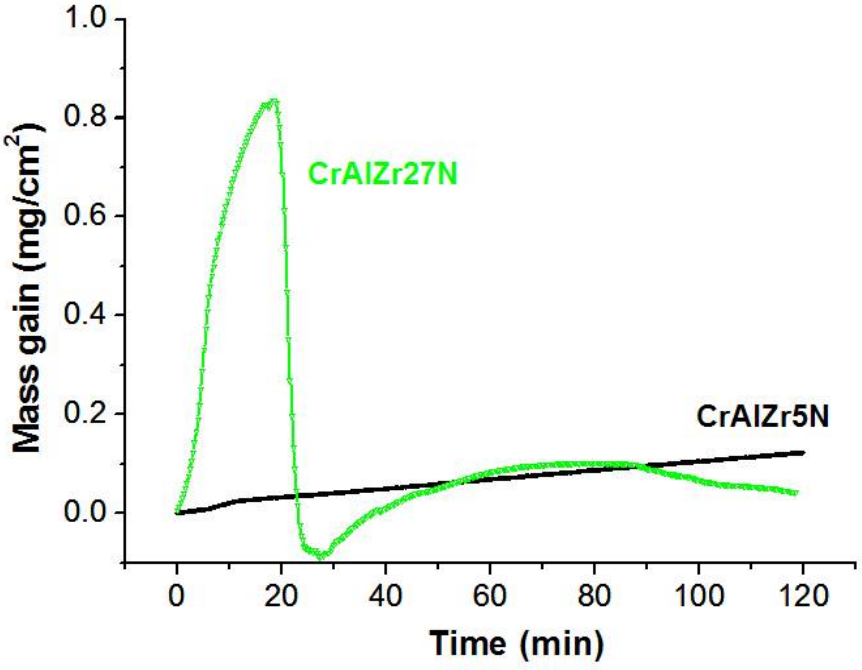

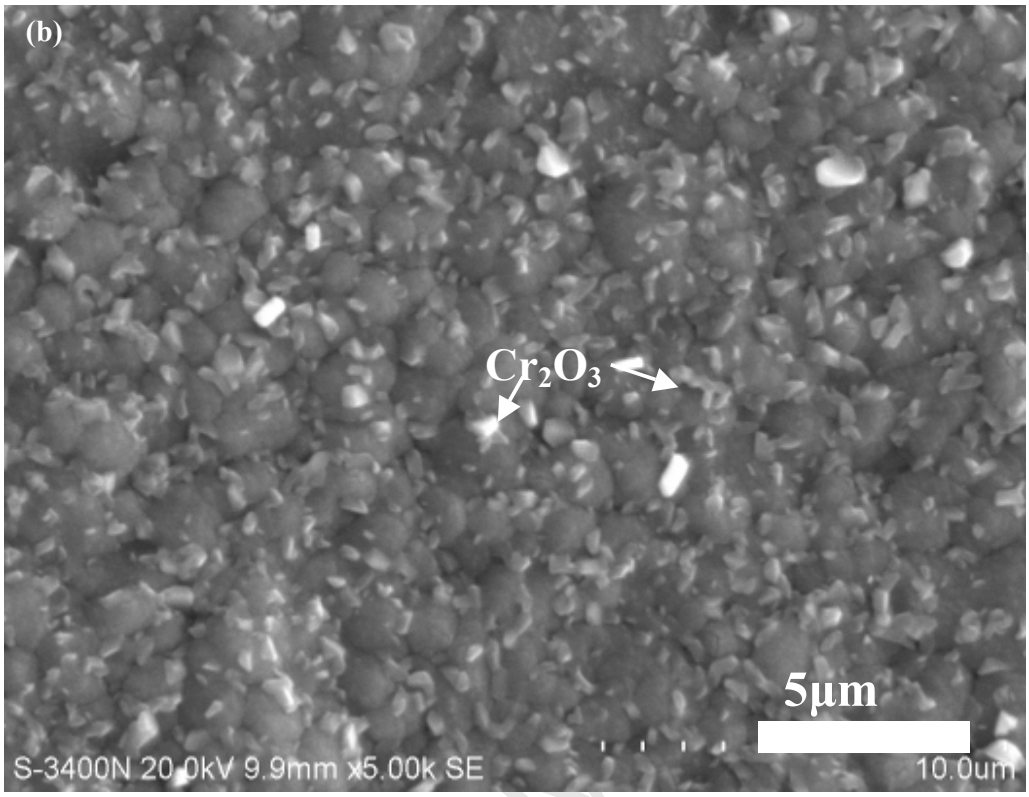

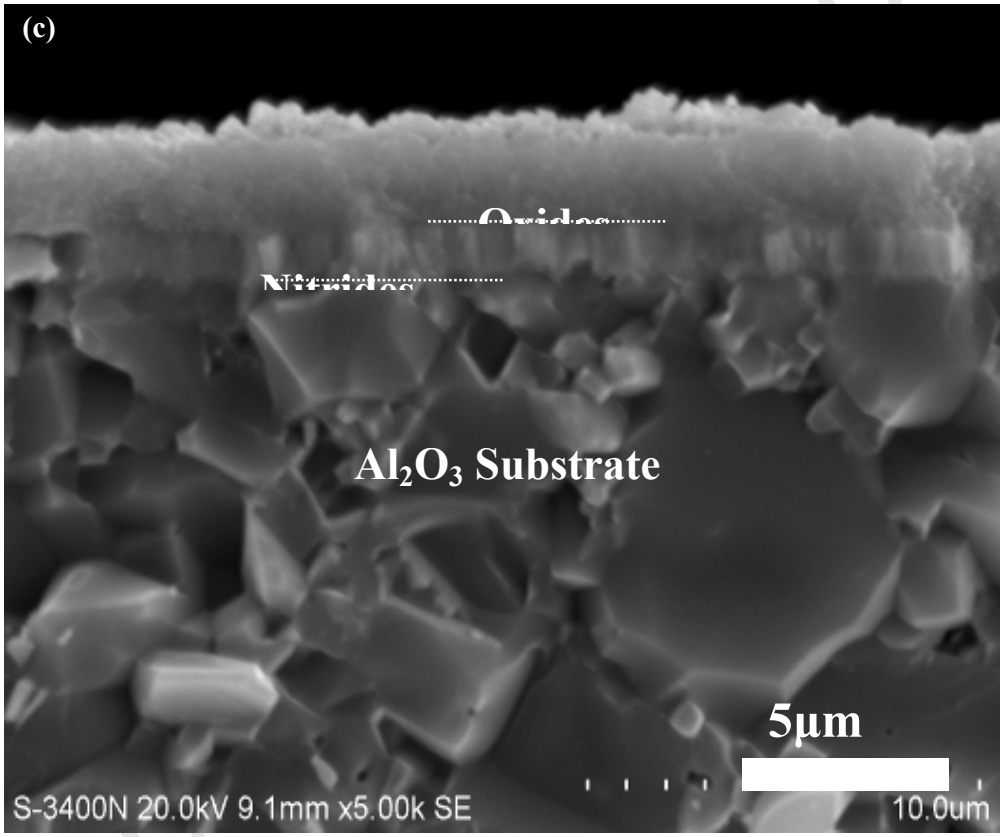

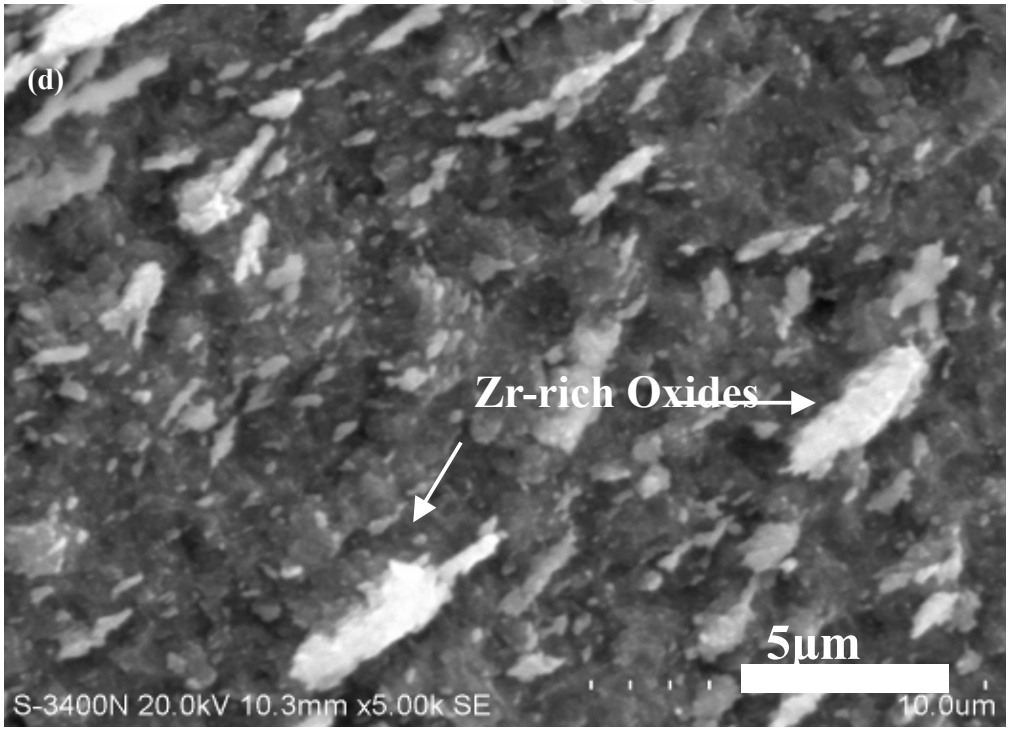

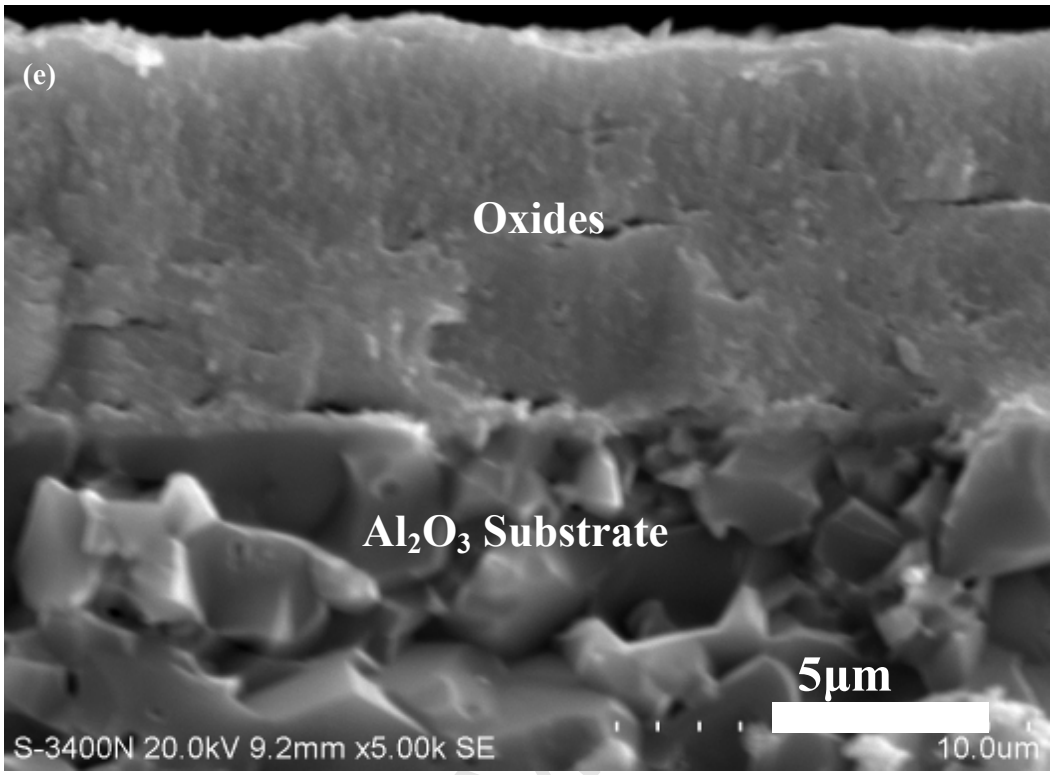

Fig. 7. TGA curves (a), SEM surface (b, d) and fracture cross-sectional micrographs (c, e) of the CrAlZr5N (b, c) and CrAlZr27N (d, e) coatings on Al_2O_3 slices after thermal exposure at 900 ^{o}C in industrial air for 2h. Oxides are Cr-rich in (c) and Zr-rich in (e), respectively; Nitrides are (Cr, Zr)N phases in (c).

(a)

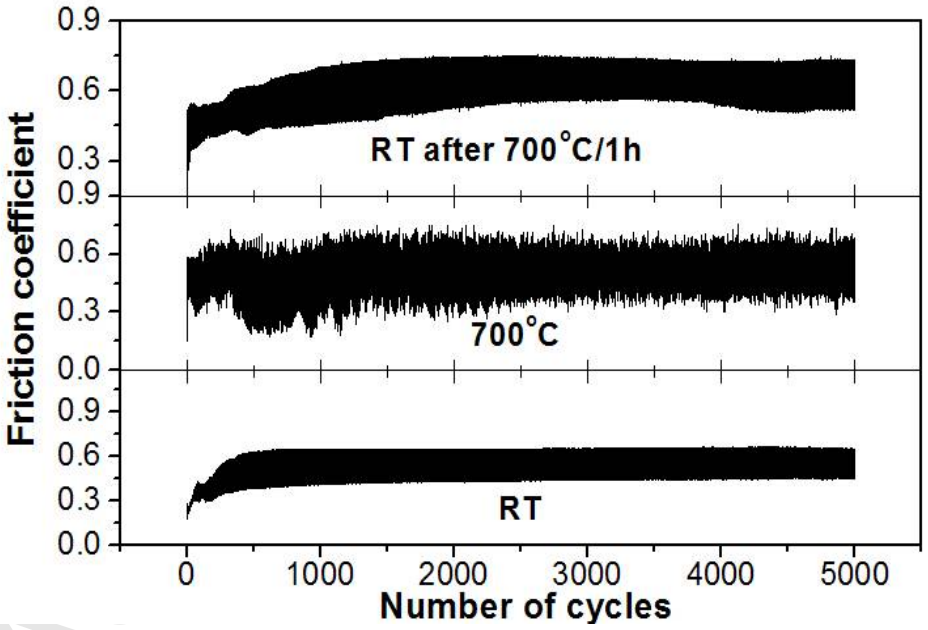

(b)

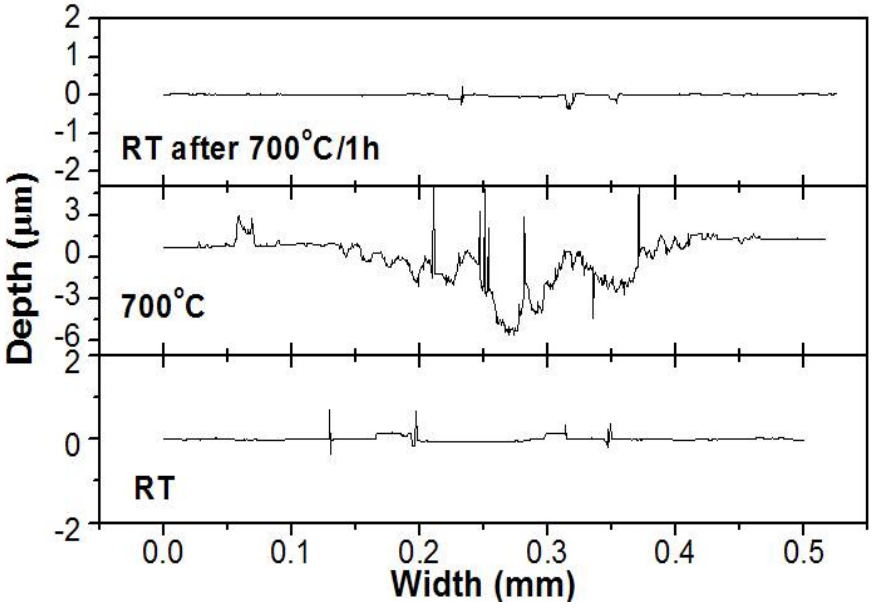

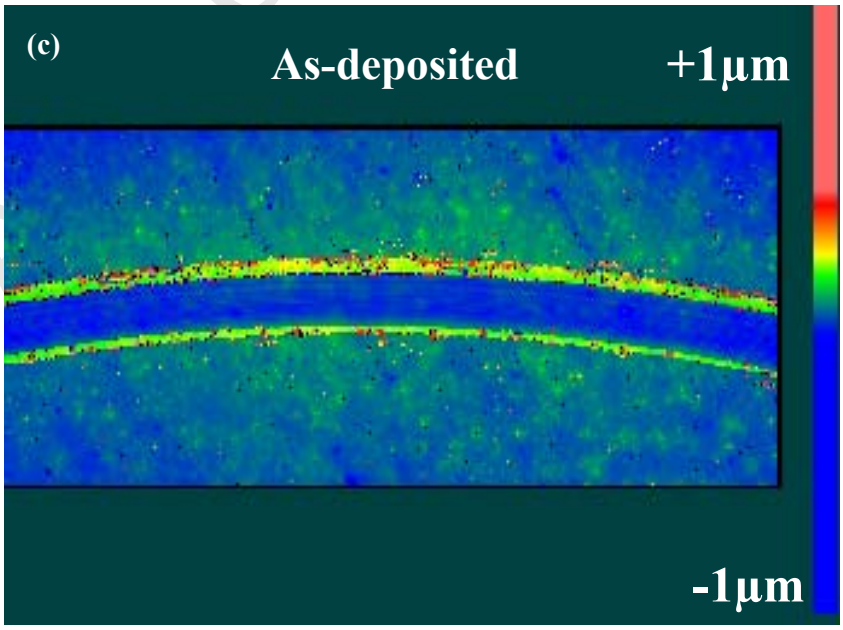

50

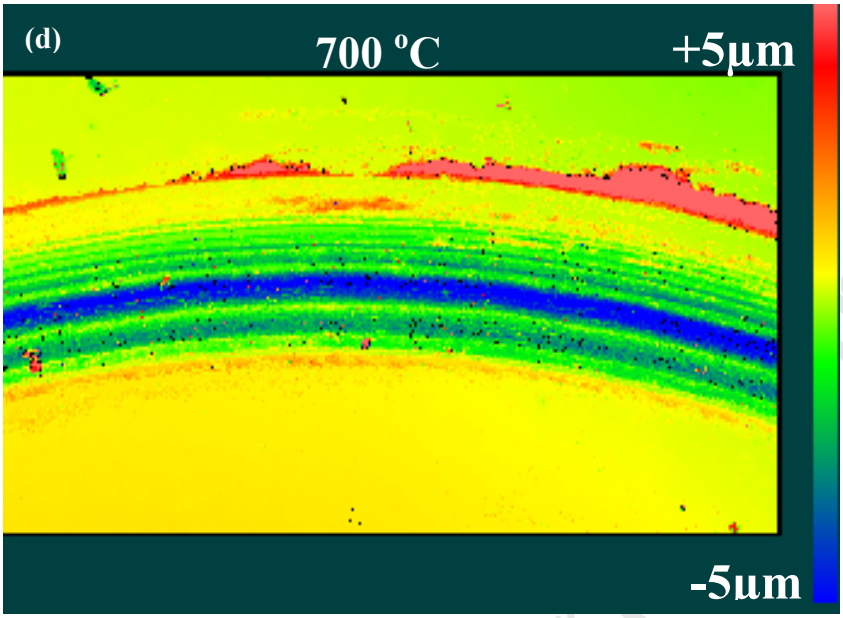

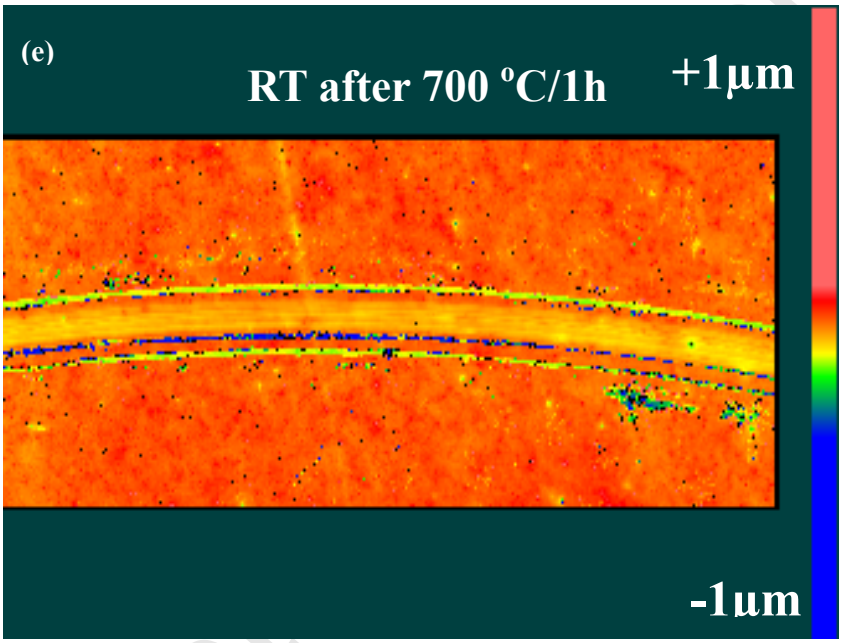

Fig. 8. Friction coefficient (a), wear track profile (b) and surface morphologies (c, d, e) of the CrAlZr5N coating on M2 steel testing under different conditions. 5 N normal applied load, 5 cm/s sliding speed and 5000 laps, and 6 mm Al_2O_3 ball as a counterpart.

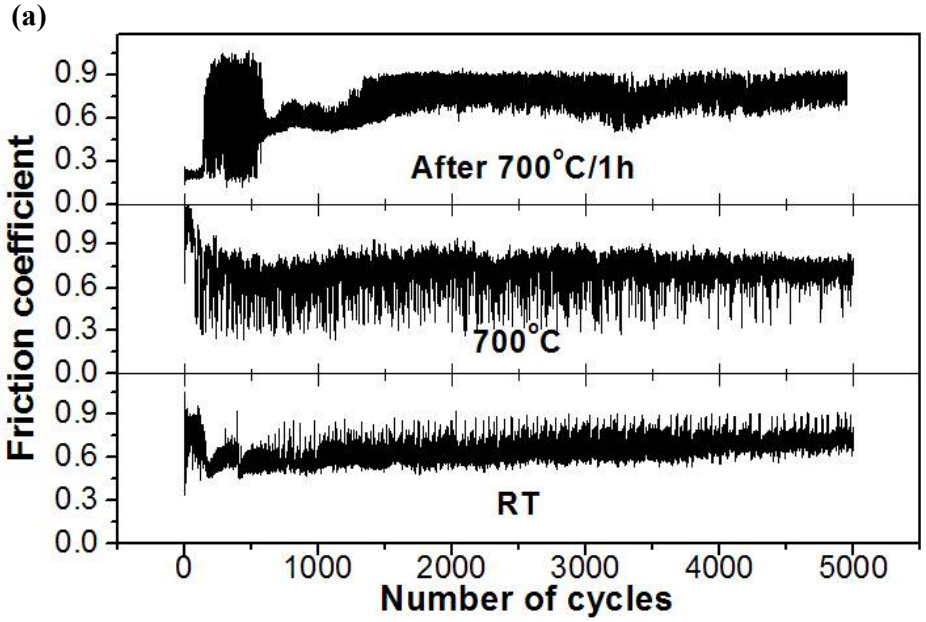

(b)

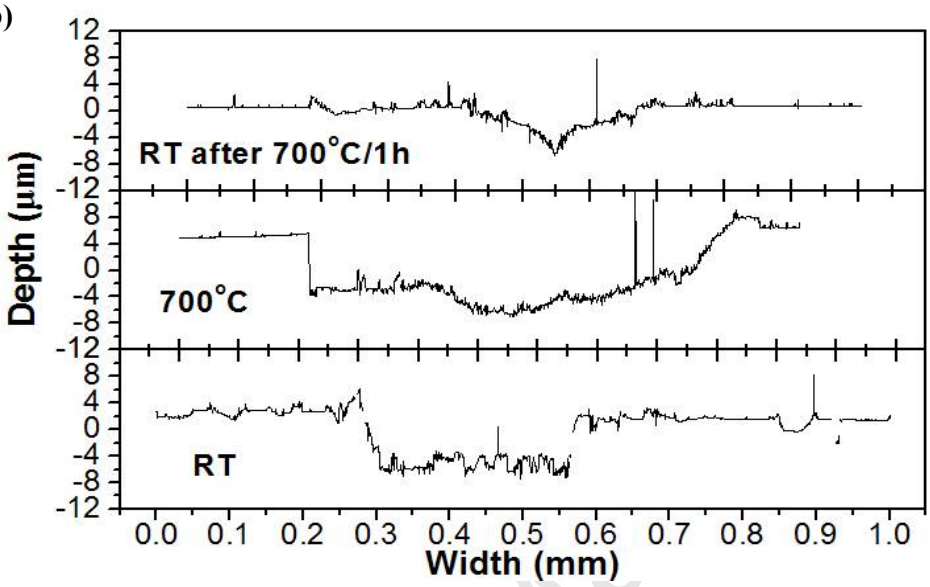

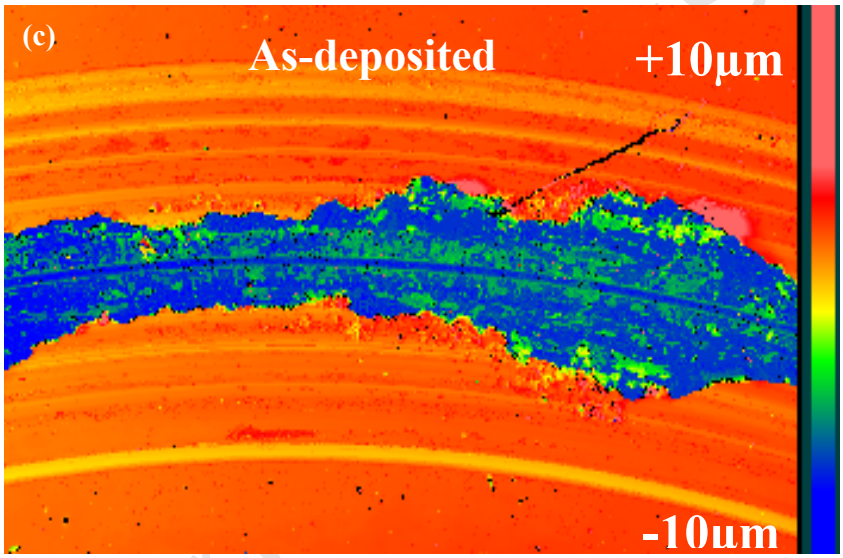

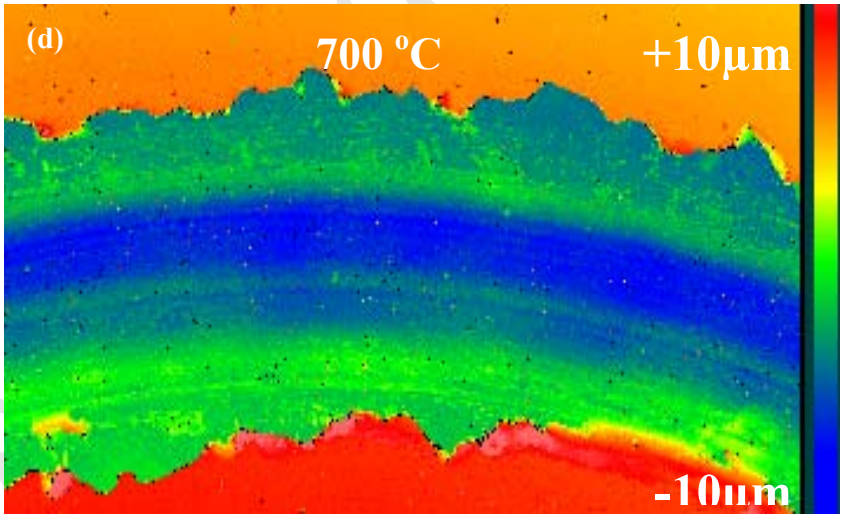

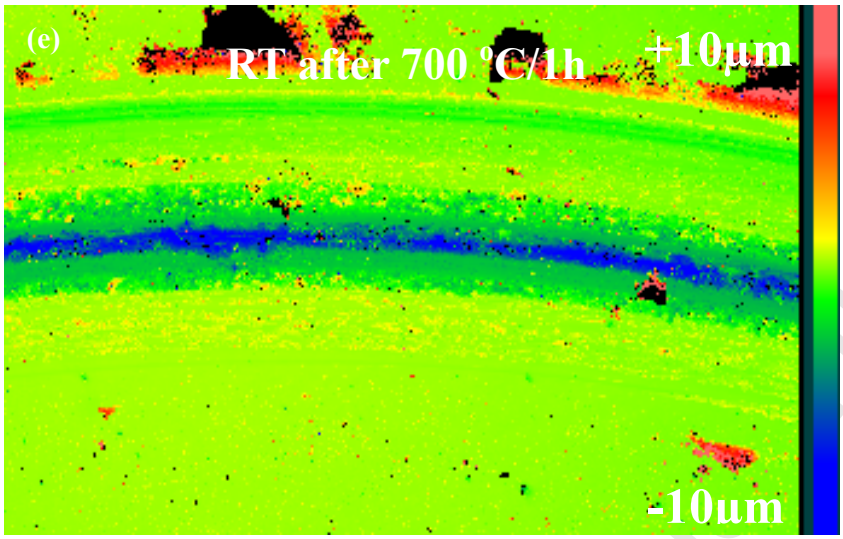

Fig. 9. Friction coefficient (a), wear track profile (b) and surface morphologies (c, d, e) of the CrAlZr27N coating on M2 steel testing under different conditions. 5 N normal applied load, 5 cm/s sliding speed and 5000 laps, and 6 mm Al_2O_3 ball as a counterpart.